# Permissible Stresses in Surface Hardened Gear Materials

**G. C. Mudd, BSc, MIMechE and J. M. France, BSc**
David Brown Gear Industries Ltd

## SYNOPSIS

*Permissible gear stresses for through hardened steels are typically presented as a simple relationship with tensile strength, but this method cannot be extrapolated to surface hardened steels. Steels of the same surface hardness may have differing permissible stresses dependent on the method of hardening. This paper rationalises these differences in terms of engineering parameters and explains the concepts behind the permissible stresses in BS 436 : Part 3.*

## INTRODUCTION

The permissible contact and bending stresses for through hardened steels are typically presented as a simple relationship with the material hardness or tensile strength. This has been found to be an adequate method for use in gear rating procedures. The method cannot, however, be extrapolated to surface hardened steels; for these steels the practice in the past has been to provide a particular permissible stress for a particular steel and hardening process.

By examining the reason why surface hardened steels differ from through hardened steels, a unified method of calculating permissible stresses has been developed and is used in BS 436 : Part 3.

The major differences are:

1. Surface hardened gears can fail from a fracture at or near the pitch line. This is because of the interaction between a contact stress (as the load line passes over the failure point) and a bending stress (when the load line is higher up the tooth flank). The bending stress is directly proportional to the load whereas Hertzian theory tells us that the contact stress is proportional to the square root of the load. Thus, because surface hardened gears carry much more load than do through hardened gears, the bending stress at the pitch line plays an increasingly important part.

2. Residual stresses are present in surface hardened steels, usually compressive at the surface, balanced by tensile stress in the region of the case/core junction. The effect of this on the perceived tooth root bending stress is to modify the mean applied stress. The effect of this on the permissible alternating stress can be explained by reference to a Goodman diagram.

3. The hardness of a surface hardened steel varies with depth below the surface. This, together with the residual stress pattern can cause a failure in the tooth root to be initiated beneath the surface of the gear. An additional tooth root bending check is therefore required.

This paper amplifies the above points and explains the premises behind the permissible stresses in BS 436 : Part 3.

## HARDENING PROCESSES

### Carburising

The fundamental feature common to all carburised components is that a carbon-rich layer at the surface is transformed to hard martensite by re-heating and quenching. The quenching process also induces a residual stress profile with compressive stress at the surface balanced by a tensile stress near the interface of case and core. Tempering then toughens the martensite with some loss of hardness and moderates the residual stress profile. Typical hardness and residual stress profiles are shown in Fig. 1.

The quality, and thus the allowable stresses of the hardened case, depends largely on the control exercised over the composition of the furnace atmosphere in order to prevent:

1. Excessive austenite retention.
2. Excessive carbide precipitation.
3. Low carbon, leading to soft non-martensitic transformation products.
4. Localised surface decarburisation.

Some measure of the importance of these factors is reflected in the values of the material quality factors, $Y_M$ and $Z_M$, in BS 436 : Part 3. For quality B materials (the specification for which includes atmosphere monitoring) $Y_M$ = 0.9 and $Z_M$ = 0.9. For the lower quality C materials $Y_M$ = 0.6 and $Z_M$ = 0.8, a reduction of 33% on allowable tooth loadings.

### Induction hardening

The induction hardening process involves inducing a high frequency current from the inductor into the near-surface regions of the tooth profile. This produces intense and extremely rapid local heating in the tooth flanks, root fillets and roots. These zones are then transformed into hard medium-carbon martensite by the quenching effects of spray jets following the inductor and the bulk oil in which the tooth being hardened is submerged.

Whilst it is possible to produce ample casedepth to suit almost any pitch of tooth, control of depth is not possible with the same degree of precision as carburise case hardening. This arises since power generator frequency has a major influence on the casedepth produced and is not a process control variable. However, provided the minimum required

G. C. Mudd is employed at David Brown Gear Industries Limited, Huddersfield. He holds a BSc (Eng) and is a Member of the Institution of Mechanical Engineers. He began his carrer in 1951 in Design, moving to Research and Development, and in 1967 was Engineering Computer Manager. In 1974 he became Chief Engineer and then, in 1978, Director of Engineering. He is currently Technical Director of the David Brown group of companies.

J. M. France joined David Brown Gear Industries in 1974 after spending eight years in the airframe industry. He holds a BSc (Eng) and has worked in various sections of the Engineering Division, including gear development testing. Currently he is supervisor of a specialist section dealing with gear technology and lubrication.

casedepth is achieved, precise control is not usually necessary. For finer pitch teeth a higher frequency energy source is necessary to provide a shallower heating effect and avoid 'back tempering' or softening of the previously hardened flank.

The residual stress profile produced is basically similar to that induced by carburise case hardening with favourable compressive stresses in the case. The balancing tensile stresses are again situated in the region of the case and core interface but typically display a higher peak value. In practice this creates no problem since the casedepth is sufficient to ensure that this peak is located in a low stress region well below the tooth surface.

As with carburising, a low-temperature temper is carried out after hardening to provide a tougher martensitic case and at the same time reduce the tensile residual stress levels. Resultant hardness is normally in the range 52/54 Rc.

### Nitriding

Nitriding differs fundamentally from the other two surface hardening process in the physical metallurgy of the hardening mechanism involved. Transformation of the hard martensite case is not involved. Instead, the inwards diffusing nitrogen combines with certain alloying elements in the steel to form small nitride particles. The high nitride case hardness is then primarily a consequence of dislocation interaction with the strain fields associated with these alloy nitrides. However, the apparent complexity of physical metallurgy belies a relatively simple, easily controllable process which can be carried out at relatively low temperature (below 550 °C) in the presence of a dissociated ammonia gas atmosphere or under plasma.

The casedepth produced is dependent on the actual composition and can be controlled by process time and, to a lesser extent, temperature. Because of limited nitrogen diffusion and reaction rates, the achievable casedepth has a maximum value of approximately 0.025 in, even with long process times. This has consequences for gear load carrying capacity which we shall examine later.

The residual stress distribution is, once again, basically similar in form to that obtained by the other processes considered, with a relatively high level of compressive stress in the case. The balancing tensile stresses tend to have peak values less than half the compressive peak. Surface hardness is primarily dependent on steel composition and to a lesser extent on prior heat treatment, specfically the tempering temperature. Naval propulsion gears have been manufactured from 3%Cr – 1%Mo steel with a surface hardness typically 850 VPN, which converts to 65 Rc.

## POST-HARDENING PROCESSES

### Grinding

One of the undesirable side-effects of the carburising process is the tendency for growth and distortion to occur. Because of this many carburised gears are finished by grinding in order to produce the required accuracy. Grinding affects the residual stress state of the carburised layer in two contrary ways. The mechanical effect (surface work hardening) induces a favourable compressive stress at the surface whilst the heat generated by the high deformation rates induces an undesirable tensile stress.

In very carefully controlled grinding operations it is possible to leave the surface with an enhanced compressive residual stress[1] but this is unlikely to be achieved under typical shop-floor conditions with conventional grinding wheels. Here, the best that can be generally expected is for the two effects to cancel each other; and unless care is taken, it is more likely that a tensile residual stress will be introduced at the surface. Because of their high thermal conductivity, CBN grinding wheels offer opportunities to induce compressive stress, but at a higher cost.

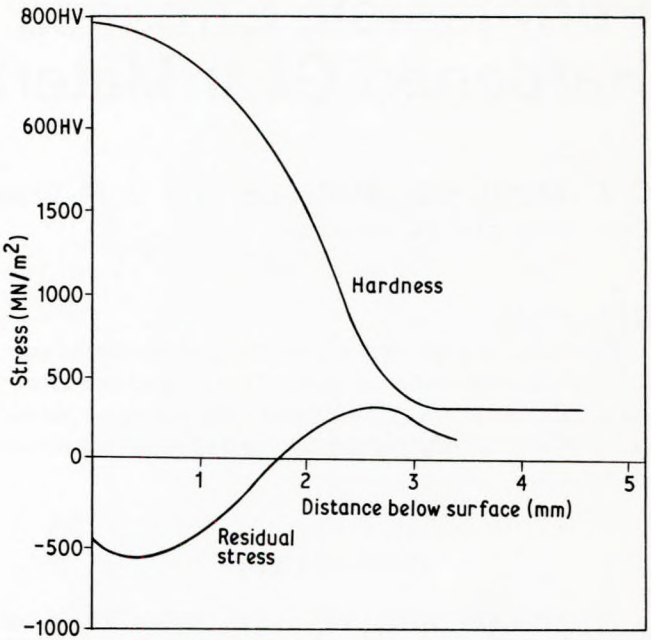


**FIG. 1: Typical hardness gradient and residual stress pattern**

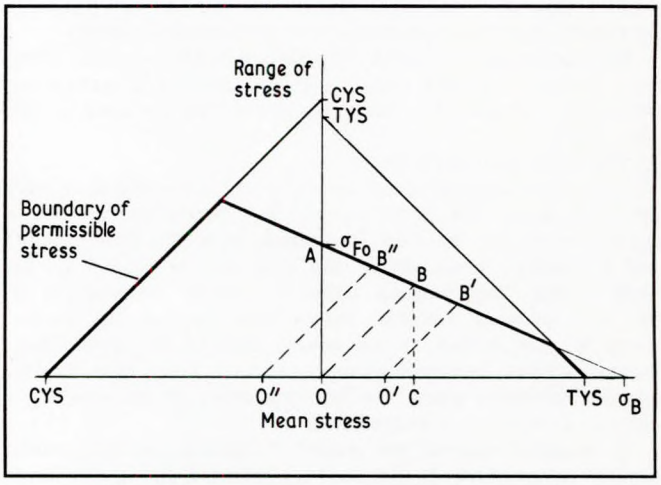


**FIG. 2 : Goodman diagram used in the analysis**

### Shot peening

In general, the effect of shot peening is to increase the surface hardness by cold working and, because the surface area is increased but remains coherent with the substrata, to induce a compressive residual stress at the surface; but in the case of carburised steel the former effect tends to be minor.

This will clearly have a beneficial effect on the permissible bending stress; also, tests by MIRA[2] indicate that shot peening tooth flanks is beneficial to the pitting resistance of carburised gear teeth. One theory put forward to explain this phenomenon is that the peened surface acts as a series of oil reservoirs, but the veracity of this is not clear.

## PERMISSIBLE STRESSES

### General

The foregoing has given an insight into the factors which may influence the permissible stresses of a carburised gear. Reference to Fig. 1 shows that the hardness and residual stress both change with the depth below the surface. Thus the

permissible stress also changes for all points at and below the surface. There is therefore a need to check the stress state both at the surface and at some point or points below the surface. The methods, which have been adopted in BS 436 : Part 3, are discussed below.

## Contact stress

### *The stress cycle for contact stress*

The stress cycle experienced by a point on the flank of a tooth consists of a compressive Hertzian stress followed by a tensile bending stress as the load moves to the tip. This clearly increases the range of stress, as originally pointed out by Mudd[3] and cited by Young.[4]

In the case of surface hardened materials the situation is further complicated due to the addition of differing residual stresses at and below the surface. The total effect of these three stresses (Hertzian, bending and residual) must then be compared with fatigue reistance of the material which (because of the hardness variation with depth in a surface hardened tooth) also varies with distance from the surface.

A computer program, HTZ, was written at DBGI to analyse fully these conditions.

A knowledge of the permissible Hertzian stress of the material (from disc tests) and the permissible bending stress (from Wohler or Schenk tests) together with HTZ could then be used to evaluate a permissible contact stress for the gear tooth, $\sigma_{Hlim}$. The program was used to analyse a wide range of gears in order to produce general curves that can be used for any gear geometry and material.

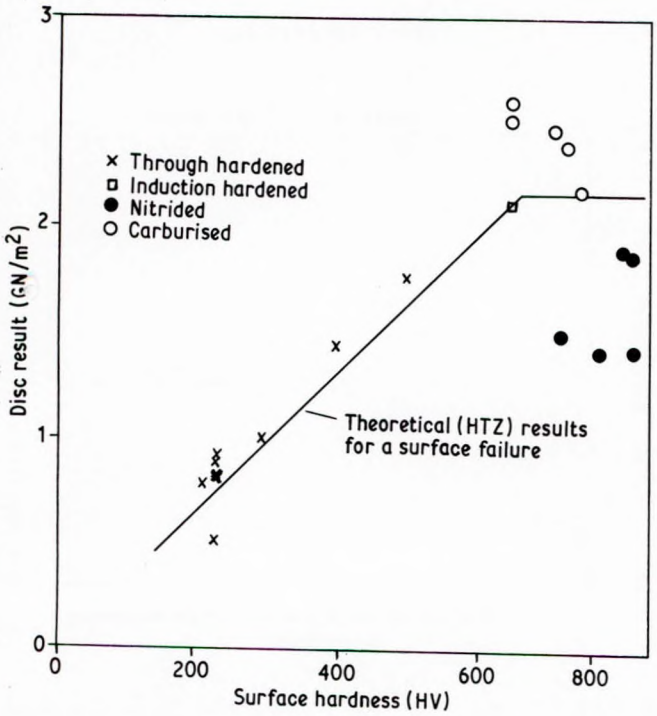


**FIG. 3: Comparison of disc results with the theoretical value for a surface failure**

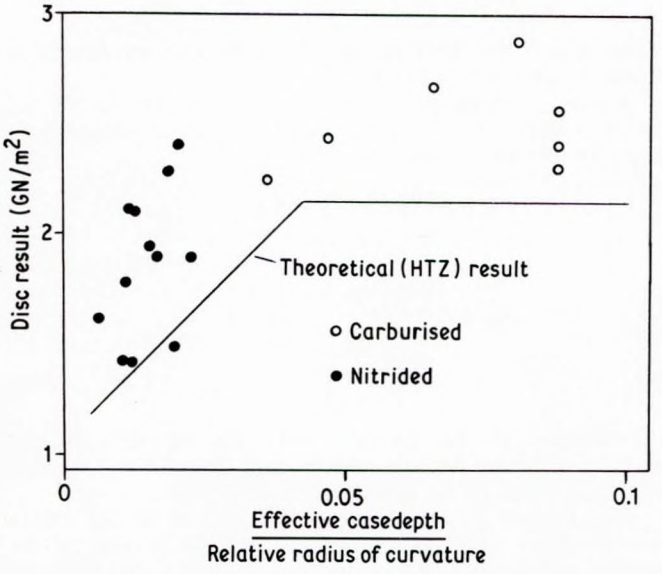


**FIG. 4: Effect of casedepth and curvature on disc results**

### *Analysis of discs*

The analysis of a disc is relatively simple compared with a gear; the only stresses involved are the applied Hertzian stress and a residual stress which varies with depth into the material. The results of disc tests are also more readily useable.

The use of accurately ground surfaces and sturdy mounting ensures that load distribution effects are minimal and the absence of a tooth contact excitation frequency precludes dynamic effects. Also important were the large number of disc test results available. Although these tests had originally been carried out to compare material performance, details of the results were still valid. HTZ was used to analyse this series of discs of different materials and casedepths based on different criteria of failure.

There are differing views as to the shape of the Goodman diagram and stress criterion that should be used. Reference to previous work[5] narrowed the field to three criteria (two direct and one shear stress), each with different Goodman diagrams. The endurance ratio was also varied for each criterion.

It was found that the criterion which best matched the experimental results was a direct stress criterion with an endurance ratio of 0.5. The Goodman diagram for this criterion is shown in Fig. 2.

When the disc results were plotted against the material hardness (Fig. 3), considerable scatter was evident at high hardness for carburised and nitrided discs. It was significant that the results below the theoretical line for a surface failure had a relatively thin casedepth because of the limitations of the nitriding process.

It was therefore decided to compare the results with the dimensionless parameter effective casedepth/radius of relative curvature (see Fig. 4). The theoretical result from HTZ is also shown on this figure.

Considering Figs 3 and 4, the horizontal portion of each graph is based on the assumption that the ultimate tensile strength becomes a maximum value of 2130 MN/m$^2$ (138 t/in$^2$) at approximately 650 $H_V$. In Fig. 4 the carburised disc results (with the exception of the one disc result on this line which was En36 with an excessive tempering temperature of 250 °C) are well above the line.

There may well be justification in extending the sloping portion of the graph to a higher level (say 2350 MN/m$^2$), or extending the line with a reduced slope for hardnesses higher than 650 $H_V$.

Again in Fig. 4, the vast majority of the results are a significant distance above the line, particularly the higher hardness nitrided discs.

This again tends to suggest the UTS should increase with hardness above 650 $H_V$, albeit at a reduced rate. In view of the relatively small amount of data involved, it has not yet been thought prudent to change what has been a long-standing practice.

## Correlation between discs and gears

Consider a tooth under the action of a load intensity $w$ at the pitch line only.

The Hertzian stress is

$$\sigma_{HD} = k_1 \sqrt{\frac{w E}{\rho_{red}}} \tag{1}$$

where $k_1$ is a constant, or

$$w = \frac{\sigma_{HD}^2 \rho_{red}}{k_1 E} \tag{2}$$

Consider now the same load intensity applied at the tooth tip. The bending stress at the pitch line is

$$\sigma_{bend} = \frac{k_2 w h_a}{t^2} \tag{3}$$

where $k_2$ is a contant, $h_a$ is the tooth addendum and $t$ is the thickness at the pitch line.

However, both $h$ and $t$ are directly proportional to the normal module, $m_n$, thus

$$\sigma_{bend} = \frac{k_3 w}{m_n} \tag{4}$$

Substituting from Equation (2)

$$\sigma_{bend} = \frac{k_4 \sigma_{HD}^2 \rho_{red}}{E m_n} \tag{5}$$

For a given material condition $\sigma_{HD}$ is constant so the bending stress is directly proportional to the ratio $\rho_{red}/m_n$. As the bending stress increases, the range of stress increases and the limiting Hertzian stress $\sigma_{Hlim}$ is reduced. Thus as the ratio $\rho_{red}/m_n$ increases the value of $\sigma_{Hlim}$ must reduce.

If $\sigma_{Hlim}$ is defined as

$$\sigma_{Him} = Z_G \sigma_{HD} \tag{6}$$

then $Z_G$, the disc/gear correlation factor, must reduce with the parameter $\rho_{red}/m_n$.

The increasing role of the bending stress can also be shown more analytically by reference to the Goodman diagram in Fig. 10 and this analysis is given in Appendix 1.

### *Analysis of gears*

Having determined the criterion of failure which best fitted the disc results, the program HTZ was then used to analyse gear teeth of various diameters and modules.

When the Hertzian stress at failure is calculated, considerable scatter arises for the same hardness carburised material.

If, however, for one particular hardness the results are plotted against the parameter $\rho_{red}/m_n$ then a clearer pattern emerges. The results for a series of hardnesses are shown in Fig. 5.

For through hardened steels with a relatively thick case the contact (Hertzian) stress at the failure load was found to correlate well when expressed as the product of the disc stress calculated previously and a factor dependent on the non-dimensional parameter radius of relative curvature/normal module, *ie*

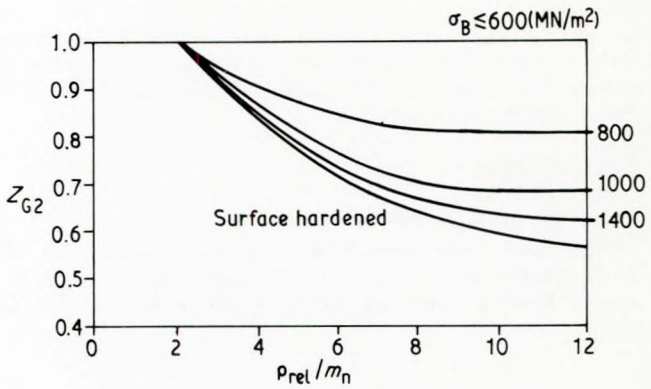


**FIG. 5: Values of $Z_{G2}$**

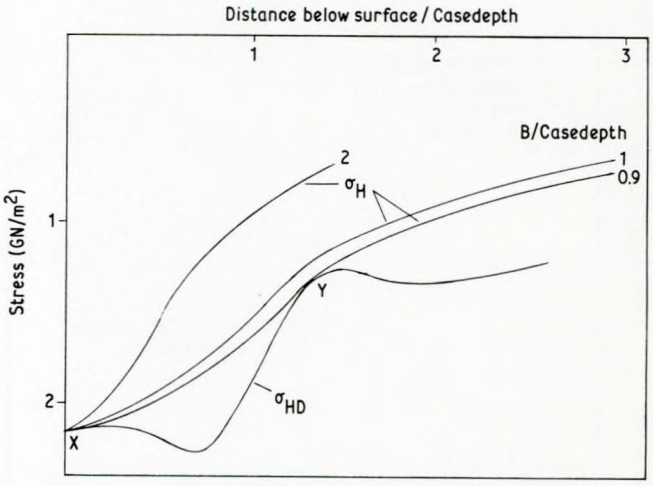


**FIG. 6: Pattern of actual and allowable stress below the surface**

$$\sigma_{Hlim} = \sigma_{HD} Z_G$$

where $\sigma_{HD}$ is the disc result and $Z_G$ is the disc/gear correlation factor as derived above (see Fig. 5).

Results of small gear tests tend to show that pinions fail before wheels. An empirical factor has been introduced to allow for this effect as follows:

$$Z_{G1} = (1.02 - 0.02\ u)\ Z_{G2} \tag{7a}$$

$$Z_{G1} = 0.9\ Z_{G2} \tag{7b}$$

whichever is the greater, where $Z_{G1}$ is the disc/gear correlation factor for the pinion and $Z_{G2}$ is the disc/gear correlation factor for the wheel, obtained from Fig. 5.

The reasons for this tendency for pinions to fail before wheels is not fully understood, but may be because of the positive addendum correction often found on pinions compared with the negative correction on wheels. This will increase the bending in pinions compared with wheels.

*Effect of thin casedepth*

For thin cases, however, as was to be expected from the disc results in Fig. 4, the above relationship did not apply. It was noted that for a given surface hardening treatment the stress increases with the casedepth up to a certain point after which further increase in effective casedepth did not cause any increase in the stress at failure. This casedepth was termed the limiting casedepth.

*Limiting casedepth (discs)*

For a disc the limiting casedepth is clearly a function of the radius of curvature. According to Equation (8) derived in Appendix 1, the failure stress for a disc is

$$\sigma_{HD} = \sigma_{comp} - \sigma_R \tag{8}$$

In Fig. 6 the allowable stress from Equation (8) has been plotted and compared with the actual stress below the surface for failures at the surface for various half-contact-bandwidths, *B*.

It can be seen that when *B*/casedepth = 0.9 the failure could occur either at the surface (point X) or sub-surface (point Y). If the casedepth falls below 0.9 then the failure will occcur sub-surface at point Y.

From classical Hertzian theory we have, for Poisson's ratio = 0.3

$$B = 1.52 \frac{w \rho_{red}}{E} \tag{9}$$

and

$$\sigma_H = 0.418 \frac{w E}{\rho_{red}} \tag{10}$$

Thus

$$\frac{\text{casedepth}}{0.9} = 1.52 \frac{w \rho_{red}}{206000} \tag{11}$$

and

$$2150 = 0.418 \frac{w\ 206000}{\rho_{red}} \tag{12}$$

Hence

$$w \rho_{red} = 107886\ (\text{casedepth})^2 \tag{13}$$

and

$$\frac{w}{\rho_{red}} = 128.43 \tag{14}$$

Equations (13) and (14) then give

$$\frac{\text{casedepth}}{\rho_{red}} = 0.035 \tag{15}$$

This is confirmed by inspection of Fig. 4.

*Limiting casedepth (gears)*

When considering a gear, however, the analysis becomes complicated because of the effect of the bending stress. As the proportion of bending stress increases, points X and Y in Fig. 6 move towards the origin, but not by the same amounts. The bending stress is a maximum at the surface, decreasing to zero at the neutral axis. Thus point X moves more than point Y and the value of *B*/casedepth at which the failure changes from the surface to sub-surface becomes less with increasing bending stress, *ie* with decreasing module for a given radius. Since the half-bandwidth, *B*, depends on the radius of curvature, the ratio of casedepth/$\rho_{red}$ is no longer constant, but changes with module. Because of the interactivity of the bending and Hertzian stresses causing changes to $\sigma_{Hlim}$ and hence the applied load and half-bandwidth, the problem has no classical solution.

The results of HTZ, however (which solves the problem using an iterative procedure), suggest that the limiting casedepth can be effectively regarded as being proportional to the module. The change with relative radius tends to be much smaller, particularly for larger $\rho_{red}/m_n$ (greater than 4), and is negligible for $\rho_{red}/m_n$ greater than 7. For smaller $\rho_{red}/m_n$ the tendency is for the radius to have an increasing effect. This is probably due to the failure being analogous to a disc, as occurs on line AE in Fig. 10 (see Appendix 1). However, this occurs when $\rho_{red}/m_n$ is less than 2, and the change has been ignored since gears in this range have very small numbers of teeth. The extra casedepth can be regarded as a safeguard in a situation where undercut and large addenduum modifications can be expected.

According to HTZ, and indeed intuition, the value of the limiting casedepth for a given gear geometry varies with the residual stress and hardness pattern induced at and below the surface of the material by heat treatment. The residual stresses and hardness used in the analysis are shown in Fig. 1.

Using these residual stresses and hardness gradients the values of limiting casedepth were:

Carburised – 0.16 times module hardened
Nitrided – 0.16 times module hardened
Induction – 0.32 times module hardened

Further examination of the results showed that, accepting the above premise, the reduction in allowable stress with casedepths less than the limiting casedepth could be plotted as a straight line relationship against the parameter actual casedepth/limiting casedepth, and that this relationship was approximately the same for the three surface hardening processes considered.

All the results could now be represented by the product of the disc stress and two factors

$$\sigma_{Hlim} = \sigma_{HD} Z_G Z_C \tag{16}$$

when $Z_C$ is the casedepth factor and

$$Z_C = \frac{5 + 3\left(\frac{\text{effective casedepth}}{\text{limiting casedepth}}\right)}{8} \tag{18}$$

*Gear tests*

The investigation was now at a stage where the program had been verified for discs, and the theoretical stresses for gears could be theoretically expressed as the product of the already proven disc stresses and two factors $Z_G$ and $Z_C$, as yet unproven.

In order to prvide experimental evidence reports of AVGRA and NAVGRA full load gear tests were examined. The major difficulty in using gear tests for comparison with theoretical results is the assessment of the load and stress modification factors: load distribution, dynamic, surface roughness, speed and velocity effects. Fundamentally based factors were used to assess these effects such as are used in the ISO and BS 436 :

Part 3. The test references, failure details and factors used are tabulated in Appendix 2.

All the test results for both discs and gears are also compared with the corresponding result from the three graphs ($\sigma_{HD}$, $Z_B$ and $Z_C$) in Fig. 7.

*Summary*

The foregoing has provided a method of calculating the limiting contact stress for gears. It reflects the change in limiting stress with:

1. The hardness and residual stress patterns of the steel.
2. The radius of relative curvature.
3. The casedepth of hardened steels.

Of these, the effect of casedepth, core hardness and residual stress pattern would merit review if more data become available.

## Bending stress

*The stress cycle for bending stress*

It has long been established[6–13] that the stress which can be withstood by an elastic material depends on the mean stress experienced and on its range of stress. The relationship is shown in the form of a Goodman diagram (see Fig. 2).

The use of this relationship allows a number of features affecting gear tooth bending strength, which could prove important to a gear designer, to be analysed.

For a component in fully reversed bending, where the mean stress is zero such as a gear tooth on an idler gear or a rotating beam test piece, the permissible alternating stress ($\sigma_{F0}$) is at point A.

For a gear tooth transmitting torgue in one direction only the mean stress is equal to the alternating stress, the locus of applied stress being OB, and the perceived permissible bending stress ($\sigma_{F0}$) is twice BC. (There are other limitations caused by tensile yield or compressive ultimate stress as shown on the diagram.)

The value of $\sigma_{F0}$ is usually established by testing the fatigue endurance ratio of a polished un-notched rotating beam. The number of cycles to failure, the condition of the surface and the size effect each have an effect on its value. These can be allowed for by the influence factors $Y_N$, $Y_R$ and $Y_X$, respectively, and therefore the generalised equation for a through hardened steel is

$$\sigma_{FP} = \frac{2\,\sigma_{F0}\,\sigma_B\,Y_N\,Y_R\,Y_X}{\sigma_B + \sigma_{F0}\,Y_N\,Y_R\,Y_X} \qquad (18)$$

A major implication from the relationship shown in Fig. 2 is the effect of a residual stress.

If a residual stress is introduced into a beam undergoing a stress cycle then the mean stress level changes. If the residual is positive or tensile then reference to the Goodman diagram shows that the locus of applied stress is O'B' and $\sigma_{FP}$ is reduced. If the residual stress is negative or compressive the locus of applied stress is O"B" and $\sigma_{FP}$ is increased. Although DP 6336 part III makes reference to this, the effect is not quantified. Using the fundamental approach it is possible to modify Equation (18) to give the following permissible stress $\sigma_{FP}$ :

$$\sigma_{FP} = \frac{2\,\sigma_{F0}\,(\sigma_B - \sigma_R)\,Y_N\,Y_R\,Y_X}{\sigma_B + \sigma_{F0}\,Y_N\,Y_R\,Y_X} \qquad (19)$$

This effect is well known and rolling or shot peening, both of which introduce a compressive residual stress near the surface, have been used as means of increasing bending strength.

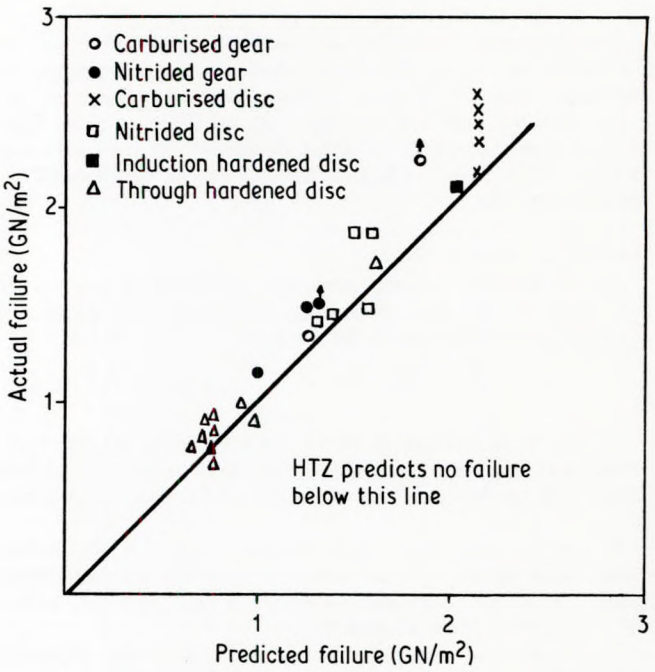


**FIG. 7: Comparison of actual and predicted failures**

*Sub-surface failure*

If the case is too thin then the sub-surface material may experience a high stress level sufficient to initiate failure before the surface stresses become critical. Equation (19) can be used to evaluate $\sigma_{FP}$ at the core by substituting $\sigma_{Bcore}$ for $\sigma_B$ and $\sigma_{Rcore}$ for $\sigma_R$. Since the material at the case/core junction is through hardened, the endurance $\sigma_{F0}$ can be assumed to be $0.5\sigma_B$ and therefore a simplification can be made to give

$$\sigma_{FP} = \frac{(\sigma_{Bcore} - \sigma_{Rcore})\,Y_N\,Y_X}{1 + 0.5\,Y_N\,Y_X} \qquad (20)$$

This permissible stress can then be compared with the actual stress at the case/core junction derived from the stress $s_F$ at the surface of the root fillet.

If $\sigma_{Fcore} > \sigma_{FPcore}$ then sub-surface failure is indicated.

## Evaluation of $\sigma_{F0}$ from tests

*General*

Starting around 1970, David Brown, the Royal Navy and Vickers Gear Research Association (NAVGRA) carried out a series of tests to determine values of $\sigma_{F0}$ for surface hardened material and to measure the associated residual stress $\sigma_R$. With these basic values established it became possible to use the basic equations developed above to calculate the permissible stress $\sigma_{FP}$ for any set of conditions. This section deals with the evaluation of $\sigma_{FP}$ and the following section with the evaluation of $\sigma_R$. The results of a series of tests to evaluate $\sigma_{F0}$ will then be presented.

The permissible value of endurance ratio for the material may be determined by testing. This may be by running gears,

by pulsator tests on notched specimens (possibly gears) or by rotating beam tests.

The are three essential stages in evaluating any bending test:

1. Evaluate the load applied to the test piece. In a gear this is affected by load distribution (tooth profile accuracy, pitch accuracy, alignment accuracy and elastic deflections) and the dynamic effects.

2. Calculate the stress level at failure from the load level, the point of application of the load, the geometry of the beam and the stress concentration effects.

3. Correct the result for the effects of differences in cycles of operation, surface texture, size, material quality, casedepth or residual stress.

The degree of confidence which can be placed in the result depends upon the accuracy of the calculation procedure used to evaluate the influence of each of the above factors. Since each factor has some error, the more factors which have to be taken into account the greater the inaccuracy. If the ISO procedure is used then the accuracy of load evaluation will depend on the accuracy of the influence factors governing load evaluation included in the standard. For example, if the load distribution factor from the procedure were 20% too low then the material permissible would be evaluated as 20% too low. The error from each of the factors compounds to give a magnified error in the material property.

*Gear tests*

When the test gears are surface hardened the same approach can be used, but there are two differences. First, a compressive residual stress is introduced into the surface layers with a corresponding tensile residual stress at the case/core junction, and secondly, as the hardness of the surface increases the endurance ratio ($\sigma_{F0}/\sigma_B$) reduces.

These differences introduce difficulties when the results are analysed. For example, depending on the process or the designer the casedepth as a proportion of the tooth thickness may vary. Also, although the surface hardness may be the same, the core hardness may vary. As mentioned above, there are some limiting values which would cause failure to occur sub-surface rather than at the surface and the effect of this may give an erroneous view of the basic material property.

Residual stress is a further source of possible error. Tests to evaluate material property must take account of these effects and therefore the calculation procedure should include them. ISO 6336 is defficient in this respect and therefore the basic material property derived using this procedure would vary depending on the finishing process, which is obviously misleading.

*Pulsator tests*

An alternative to using gears as the test specimen is to use a pulsator. Some of the uncertainties of load determination are removed since the pulsator machine can be calibrated to within 1 or 2%. The level of stress is determined with more precision because the point of application of the load can be controlled and is not subjected to the vagaries of tooth profile, pitch or alignment accuracies. The value of the stress concentration factor is usually evaluated by finite element analysis or, if the test piece is a gear tooth, possibly by the ISO procedure.

**Table I: Residual stresses - carburised test gears**

| | *Residual Stress* (MN/m$^2$) | |
|---|---|---|
| | $\sigma_{Rmax}$ | $\sigma_{Rmin}$ |
| Shaved flank | -265 | -330 |
| Ground flank | +26 | -242 |
| Shot peened flank | -771 | -825 |
| Ground root | +275 | +147 |

There seems to be little to choose in this respect between test pieces such as the Schenck, described later, or static gear teeth. The latter has a cost advantage in that one gear can provide many test pieces.

*Rotating beam tests*

Here the uncertainties are reduced to a minimum. The load applied and the stress level has a high level of confidence and for through hardened or normalised materials this must be the simplest and most effective means of deriving material properties.

When the rotating beam tests are used for surface hardened materials there is a problem caused by the residual stress pattern.

This can be resolved by making the rotating beam specimens of case material only. This has an added advantage in that, being homogeneous, there is no residual stress. The test result can therefore be taken as a direct value of $\sigma_{F0}$ with no correction calculation required.

## RESIDUAL STRESS TESTS

Levels of residual stress in surface hardened items are usually measured by one of two principal methods:[14] (a) experimentally relieving the locked-in stresses and measuring the strain which results or (b) using an X-ray diffraction technique. The measurement of residual stresses in gear teeth was studied by the NAVGRA organisation in 1976,[15] which recommended the use of the X-ray diffraction method, coupled with chemical machining for controlled surface layer removal.

### Carburised gears

This method was then chosen[16] to investigate three different pitches milled from identical tests blocks. The teeth were undercut to simulate protuberance hobbing and, after carburising and hardening, the flanks were ground.

These results showed a high stress level in the immediate vicinity of the surface which was associated with a reduction in the percentage of austenite near to the surface. This would not have been disclosed by the deflection measurement technique. However, a generally similar pattern of stress distribution was demonstrated for the three pitches examined. The residual stresses on the ground flanks were less compressive than on the unground root. Apparently the magnitude of the change was affected by the pitch and therefore may be associated with the degree of heat generated in the surface by the grinding process.

Later, using the same technique, measurements were carried out for David Brown by the British Steel Corporation[17] on three carburised and hardened gears, each finished by a different surface treatment:

1. Hobbed,shaved and carburised.
2. Hobbed, carburised and ground.
3. Hobbed, carburised, ground and shot peened.

The result of these measurements, which were for the surface only, are as shown in the Table I.

Although the value of compressive residual was smaller than the peak values found in the previous tests, these results show a similar general pattern. The unground surface has a compressive residual which is then modified by grinding such that the $\sigma_{Rmax}$ is just tensile. The ground root had a higher tensile stress than the flank, and although this is not fully understood it may be caused by the greater grinding feed in the root region compared with that on the flank.

Other measurements[18] on the unused flanks of case hardened and ground 1 m diameter gear teeth showed similar patterns. Measurements were taken on the drive flanks after running and on the unused flanks. The values obtained also indicate that the grinding on the flank reduces the compressive residual near to the surface. However, high negative values were measured near the surface on the drive flanks.

**Table II: Pulsator test results on carburised Schenck specimens**

| Report no. | No. of specimens | Material | HT | Case depth | VPN | RA (%) | $\sigma_B$ (MN/m$^2$) | $\sigma_R$ (MN/m$^2$) | $\sigma_{Flim}$ (MN/m$^2$) | $Y_S$ | $\sigma_F$ (MN/mm$^2$) | $\sigma_{FO}$ (MN/mm$^2$) |
|---|---|---|---|---|---|---|---|---|---|---|---|---|
| 72/15/3 | 9 | 655M13 | carb | 2.01 | 679 | 17 | 2130 | -400 | 635 | 1.4 | 889 | 639 |
| 72/15/4 | 12 | 655M13 | carb | 1.73 | 670 | 16 | 2130 | -400 | 624 | 1.4 | 874 | 626 |
| 72/24/1 | 12 | 655M13 | carb | 2.08 | 722 | | 2130 | -400 | 704 | 1.4 | 986 | 725 |
| 72/24/2 | 12 | 655M13 | carb | 2.03 | 703 | | 2130 | -400 | 571 | 1.4 | 800 | 563 |
| 72/7/1 | 12 | 655M13 | carb | 1.68 | 737 | | 2130 | -400 | 619 | 1.4 | 867 | 620 |
| 73/7/2 | 12 | 655M13 | carb | 1.73 | 722 | | 2130 | -900 | 764 | 1.4 | 1070 | 643 |
| 75/4/2 | 8 | 655M13 | carb | 1.75 | 707 | 17 | 2130 | -400 | 645 | 1.4 | 903 | 651 |

## DETERMINATION OF $\sigma_{F0}$

Carburised and hardened specimens were tested on a Schenck machine by NAVGRA[19–22] over a number of years. A summary of some of the results is given in Table II, from which the value of $\sigma_{F0}$ can be evaluated. Inverting Equation (19) gives

$$\sigma_{F0} = \frac{\sigma_{FP}\,\sigma_B}{\left(2\sigma_B - 2\sigma_R - \sigma_{FP}\right) Y_N\, Y_R\, Y_X\, Y_M} \qquad (21)$$

Note that, since the value of $\sigma_{F0}$ is required for a high-quality material, a factor has been introduced to take into account the quality of the specimens, which in these tests was a commercial quality case hardening steel. This factor has been designated $Y_M$.

The value of $Y_S$ used was derived using finite element analysis. Two different types of specimen were used, hence two values of $Y_S$ are given in Table II.

For these tests $Y_N$ = 1.0, $Y_X$ = 0.84, $Y_R$ = 0.94, $Y_M$ = 0.9, and $Y_\delta$ = 1.0.

These results indicate an endurance ratio of between 0.25 and 0.29. This is dependent on the accuracy of the assumptions made in the analysis. It seems low compared with the two following test examples, also conducted by NAVGRA[20] on carburised materials.

### Rotating beam tests

A series of tests was conducted by David Brown[23] using homogeneous rotating beam specimens made from the equivalent of 655M13 case materials after carburising, with different carbon levels. Eight groups of specimens were used, each having fifteen test pieces.

The results are variable and have a range of endurance ratios between 0.3 and 0.44. This is considerably higher than the endurance ratio from the pulsator tests. The finite life part of the life curves is not well defined, but the 'knees', where discernible, lie between 3 x $10^5$ and 4 x $10^6$, with the majority at the high value.

### Avery pulsator test

The original objective was to compare results from two groups of notched test pieces, one of which had the notch machined into the commercial quality material and the other had the notch hot-formed. The hot-formed notch was dressed to the same size as the machined notch.

All the specimens from both groups were heat treated together giving an affective casedepth of 1.8 – 2.0 mm with a surface hardness of 695 VPN. The $\sigma_{Flim}$ was 679 and 664 MN/m$^2$, respectively, giving endurance ratios of 0.32 and 0.31. Interestingly, there was little apparent advantage from the forged notch.

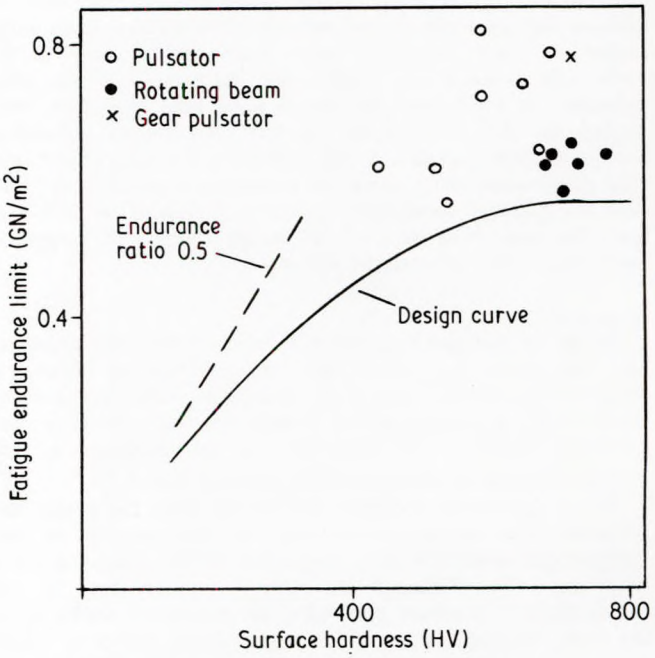


**FIG. 8: Design values and test results for bending stress**

### Gear tooth pulsator tests

As a further comparison, a series of pulsator tests were carried out on a 5 mm module carburised and ground test gear. In each test two teeth (14 teeth apart) were loaded by two anvils clamped in the upper and lower collets. The rig was calibrated statically by means of a load cell, the output of which was compared with the continuous read-out built into the machine. High and low cycle fatigue tests were carried out.

In total twenty-six gear teeth were tested at many different load levels, twenty-three of which failed. The fatigue endurance limit was 1180 MN/m$^2$. Assurming $\sigma_R$ = - 400 MN/m$^2$, $Y_M$ = 0.9, $Y_O$ = 1.03, $Y_R$ = 0.9, $Y_X$ = 1.0, the calculated value of $\sigma_{F0}$ = 795 MN/m$^2$, giving an endurance ratio of 0.37.

### Generalised permissible values

The results described above are shown in Fig. 8. The significant points to be made are:

1. There is a large amount of scatter. This is not unusual in fatigue testing, but here it seems to be particularly dispersed.

2. There is always the possibilty that the variability of the results may be caused by the variability introduced by the process rather than a basic material variability. The fatigue value is known to be adversely affected by a high percentage

of retained austenite,[12] inter-granular oxidation, and decarburisation, all of which result from poor control of the hardening process.

3. For this reason a design curve must be well below the mean curve. The design curve in BS436 : Part 3 is shown in Fig. 8.

The value for 700 $H_V$ and above is a constant although this has largely been influenced by the Schenck results. If these were ignored a continued increase of $\sigma_{F0}$ with VPN is indicated and this may be an important area of future investigation.

## CONCLUSIONS

This paper has explained the premises behind the permissible stresses in BS 436 : Part 3. In particular, it has shown:

1. How bending at the pitch line combines with the contact stress to increase the range of applied stress at the pitch line.

2. How residual stresses induced by surface hardening processes and modified by post-hardening processes affect both contact and bending stresses.

3. How the radius of relative curvature and module affect the contact stress.

It has also summarised the various methods used to measure permissible stresses and concludes that the tests on specimens of simple geometry are to be preferred to gear tests.

## REFERENCES


1. M.W.Gormley, 'Residual grinding stresses. Grinding stresses - cause, effect and control, 7-21'. Collected paper published by Grinding Wheel Institute (USA).
2. H.C.Allsopp, and R.J. Love, 'Resistance to pitting of gear teeth - a comparison of gear production processes'. The Motor Industry Research Association (March 1958).
3. G.C. Mudd, 'A numerical means of predicting the fatigue performance of nitride-hardened gears'. *Proc. I. Mech. E.* (Sept. 1970).
4. I.T.Young, 'A wider scope for nitrided gears.' *GEC Journal of Science and Technology*, Vol. 46, no.3. (1980).
5. A. Rhodes, 'Interim report on theoretical fatigue. Failure criteria, based on correlation with disc test results'. Unpublished DBGI report.
6. C. Lipson and R.C. Juvinall, *Handbook of Stress and Strength* (Macmillan Company, New York, 1963).
7. N.H. Polakowski and E.J. Ripling, *Strength and Structure of Engineering Materials* (Prentice-Hall Inc., Englewood Cliffs, NJ, 1966).
8. P.G. Forrest, *Fatigue of Metals* (Pemmgamon Press, Oxford, 1962).
9. T.V. Duggan and J. Byrne, *Fatigue as a Design Criterion* (Macmillan Press Ltd, Basingstoke, 1977).
10. R.J. Roark and W.C. Young, *Formulas for Stress and Strain* (McGraw-Hill Inc., New York, 1938).
11. N.E. Frost et al., *Metal Fatigue* (Oxford University Press, Oxford, 1974).
12. B.I Sandor, *Fundamentals of Cycle Stress and Strain* (University of Wisconsin Press, 1972).
13. H.J. Gough, *The Fatigue of Metals* (Ernest Benn Ltd, London, 1926).
14. J.O Almen, and P.H. Black, *Residual Stresses and Fatigue in Metals*, chapter 7 (McGraw-Hill Inc., New York).
15. S. McEwan and D. Martin, 'Evaluation of techniques for residual stress measurement with paritcular reference to gear teeth'. NAVGRA Report 76/1
16. D. Martin and R.G. Nicholl, 'The measurement of residual stress and retained austenite in case hardened specimens of simple form and in case hardened rack teeth of pitch sizes'. NAVGRA Report 78/3.
17. B.S.C. Report RSC/7320/84, 'The residual stress evaluation of surface treatments'.
18. B.S.C. Report RSC/7464/85, 'The through thickness variation of residual stress in En 36 gears'.
19. S. McEwan, B. Egan and G. Dunderdale, 'Schenck tests - Effects of core strength and tempering tempeerature on the bending fatigue strength of carburised and hardened En 36 steel. Part 1 - Core strength investigation at 150 °C tempering temperature'. NAVGRA Report 72/15.
20. S. McEwan, B. Egan and D.R. Lacey, 'Schenck tests - Investigation into the effect of grain directionality on the bending fatigue strength of En 36 carburised and hardened material'. NAVGRA Report 72/14.
21. S. McEwan, B. Egan, and G. Dunderdale, 'Schenck tests - Effect of vapour blasting and shot peening on the bending fatigue strength of carburised and hardened En 36 steel'. NAVGRA Report 73/7.
22. S. McEwan, B. Egan and G. Dunderdale, 'Comparison tests on MK1A, MK11W and MK11UW Schenck specimens to allow correlation of results from the different types of specimens'. NAVGRA Report 75/4.
23. J.M. Chaney, 'The bending resistance of 8 carburised case elements of a 3% Ni-Cr carburising steel'. Internal DBGI Report H/R/24V.


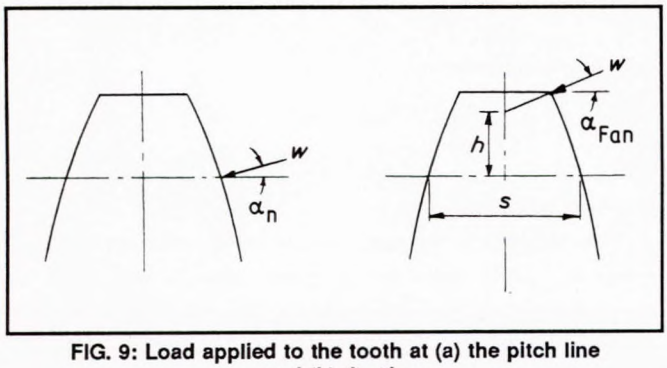


**FIG. 9: Load applied to the tooth at (a) the pitch line and (b) the tip**

## APPENDIX 1

### An analysis of the effect of bending stress at the pitch line

Consider the stress cycle at the reference diameter of the tooth as the load moves up the flank to the tip [Fig. 9 (a and b)].

The Hertzian stress when the load is at the point under consideration is

$$\sigma_{Hlim} = \frac{189.7\ w}{\rho_{red}} \tag{21}$$

or

$$w = \frac{\sigma_{Hlim}^2\ \rho_{red}}{35990} \tag{22}$$

When the load moves to the tip the bending stress parallel to the tooth axis is

$$\sigma_b = \frac{6\ w\ h\ \cos\alpha_{Fan}}{s^2} \tag{23}$$

Then the bending stress parallel to the tooth surface (in the same direction as the Hertzian stress) is

$$\sigma_b = \frac{6\ w\ h\ \cos\alpha_{Fan}}{s^2}\left((1+\nu)\cos^2\alpha_n - \nu\right) \tag{24}$$

But, ignoring backlash

$$s = \frac{\pi m_n}{2} \tag{25}$$

Hence

$$\sigma_b = \frac{24\, w\, h \cos \alpha_{Fan}}{\pi^2 m_n^2} \left( (1 + \nu) \cos^2 \alpha_n - \nu \right) \tag{26}$$

Substituting for $w$ from Equation (22)

$$\sigma_b = \frac{\sigma_{Hlim}^2 \rho_{red}\, h \cos \alpha_{Fan}}{1500\, \pi^2 m_n^2} \left( (1 + \nu) \cos^2 \alpha_n - \nu \right) \tag{27}$$

Consider now the equations of the loading and of the various sections of the Goodman diagram shown in Fig. 10.

The mean and alternating stresses applied to the tooth are

$$\sigma_M = \frac{\sigma_b + \sigma_H}{2} + \sigma_R \tag{28}$$

and

$$\sigma_A = \frac{\sigma_b - \sigma_H}{2} \tag{29}$$

where $\sigma_A$ is the alternating stress, $\sigma_b$ is the bending stress, $\sigma_H$ is the Hertzian stress, $\sigma_M$ is the mean stress and $\sigma_R$ is the residual stress.

The equation of AB is

$$\sigma_A = \sigma_M - \sigma_{comp} \tag{30}$$

where $\sigma_{comp}$ is the ultimate compressive strength.

Substituting Equations (28) and (29) in Equation (20) gives

$$\sigma_H = \sigma_{comp} - \sigma_R \tag{31}$$

Hence the failure is independent of the bending stress and this accounts for the horizontal line on the $Z_G$ curve.

As the module decreases the failure moves to BC where

$$\sigma_A = \frac{\sigma_B - \sigma_M}{2} \tag{32}$$

where $\sigma_B$ is the ultimate tensile strength.

Substituting from Equations (28) and (29) gives

$$\sigma_H = 3\, \sigma_b - 2\, \sigma_B + 2\, \sigma_R \tag{33}$$

Then substituting for $\sigma_b$ from Equations (27) and (33) yields a quadratic equation in $\sigma_{Hlim}$ of the form

$$k_1 \sigma_{Hlim}^2 + k_2 \sigma_{Hlim} + k_3 = 0 \tag{34}$$

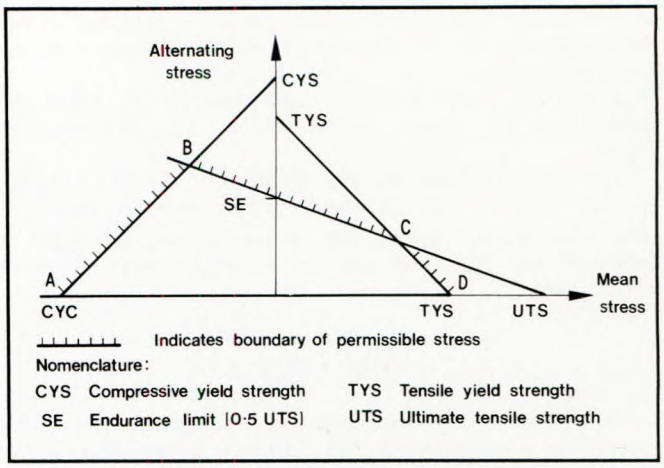


**FIG. 10: Goodman diagram used in the analysis**

where

$$k_1 = \frac{\rho_{red}\, h \cos \alpha_{Fan}}{1500\, \pi^2 m_n^2} \left( (1 + \nu) \cos^2 \alpha_n - \nu \right) \tag{35}$$

$$k_2 = -1 \tag{36}$$

$$k_3 = 2\left(\sigma_B - \sigma_R\right) \tag{37}$$

The computer program evaluates the stress situation thoroughly but in order to illustrate the form of the equation, consider the case of a 20° gear with $\nu = 0.3$ and for simplicity let $h = m_n$.

Then

$$k_1 = \frac{\cos \sigma \alpha_{Fan}\, \rho_{red}}{5280\, m_n} \tag{38}$$

and the value of $\sigma_{Hlim}$ becomes

$$\sigma_{Hlim} = \frac{1 - \sqrt{1 + \dfrac{\cos \alpha_{Fan}}{727} \dfrac{\rho_{red}}{m_n} \left(\sigma_B - \sigma_R\right)}}{\dfrac{\cos \alpha_{Fan}}{2910} \dfrac{\rho_{red}}{m_n}} \tag{39}$$

subject to a minimum of

$$\sigma_{Hlim} = \sigma_{comp} - \sigma_R \tag{40}$$

governed by line AB.

The variation in cos $\alpha_{Fan}$ for different tooth geometries is relatively small, thus for a given material ($\sigma_B$ and $\sigma_R$ constant) $\sigma_{Hlim}$ is dependant upon $\rho_{red}/m_n$, and has a shape of the form shown in Fig. 5.

## APPENDIX 2

### Tabulation of DBGI results

The results are given in Table III. Note that all tests were performed on 4 in diameter discs with 2 in diameter rollers, *ie* relative radius of curvature = 0.6667 in (16.93 mm).

**Table III: DBGI results**

| Failed Element | Material | UTS (MN/m²) or HV | Effective Casedepth (mm) | $\sigma_{HD}$ (MN/m²) | Report Ref. |
|---|---|---|---|---|---|
| Disc | En9 | 772 | | 895 | H/R/.26E |
| Disc | En8 | 649 | | 765 | H/R/.26G |
| Roller | En8 | 710 | | 867 | H/R.26G |
| Disc | En9 | 772 | | 695 | H/R/26H |
| Disc | En9 | 772 | | 803 | H/R/26J |
| Disc | En9 | 772 | | 672 | H/R26K |
| Disc | En25 | 933 | | 951 | H/R/266 |
| Disc | En30A | 1270 | | 1346 | H/R.26N |
| Disc | En30B | 1606 | | 1720 | H/R/26O |
| Disc | En25 | 958 | | 900 | H/R/26P |
| Disc | En24IH | 639HV | 4.6 | 2077 | H/R/26V |
| Roller | En36CH | 740HV | 1.5 | 2328 | H/R/26.21 |
| Roller | En36CH | 720HV | 1.5 | 2417 | H/R/26.21 |
| Roller | En36CH | 640HV | 1.5 | 2944 | H/R/26.21 |
| Roller | En36CH | 640HV | 1.5 | 2568 | H/R.26.21 |
| Roller | En36CH | 780HV | 1.5 | 2134 | H/R/26.21 |
| Disc | En40CNit | 880HV | 0.15 | 1409 | H/R/26.12 |
| Disc | En40CNit | 860HV | 0.25 | 1869 | H/R/26.12 |
| Disc | En40CNit | 850HV | 0.36 | 1884 | H/R/26.12 |
| Disc | En40CNit | 744HV | 0.30 | 1489 | H/R/26.13 |
| Disc | En40CNit | 810HV | 0.19 | 1398 | H/R/26.15 |

## APPENDIX 3

### Tabulation of AVGRA and NAVGRA test results and factors used

All AVGRA and NAVGRA test reports were examined and Table IV shows the results and factors produced. En36 and En40 results are plotted in Fig. 6 as failures when the failure was due to pitting or fracture at the pitch line with the exception of the tests cited in 1 to 5 below. If the failure was due to other causes than the mating element (if undamaged) has been plotted as unfailed. The following results were rejected for the reasons given:

1. AVGRA 2DP (RD0710) - The wheel pitting was not progressive, metalurgical examination of the pinion showed the steel to be 'dirty'.

2. AVGRA 2DP (RD0708) - Pinion wobble caused high end loading, soft areas were found where the pitting occurred.

3. NAVGRA 6DP (76/8) - The white layer on the wheel was considered too deep.

4. AVGRA 3DP (W14) - Meshing difficulties caused overloading at the untorqued end where the failure occurred.

5. NAVGRA 12DP (68/14) - The wheel fracture was attributed to the wheel manufacture (radial screwed pegs and caulking).

**Table IV: AVGRA and NAVGRA scale gear tests**

| *Test Ref* | *Failure Details* | | | *Pinion* | | | *Wheel* | | |
|---|---|---|---|---|---|---|---|---|---|
| | Power(kW) | Speed | Failure description | Material[1] | $Z_c$ | $\sigma_{HD}Z_G^2$ | Material[1] | $Z_c$ | $\sigma_{HD}Z_G^2$ |
| AVGRA 4DP (RD0711) | 11930 | 1500 | Pinion fracture, PL | En36 | 1.00 | 1334 | En36 | 1.00 | >1334 |
| AVGRA 2DP (RD0712) | 17900 | 1500 | Pinion pit after scuffing | En36 | 1.00 | 1404 | En24 | 1.00 | >1404 |
| AVGRA 2DP (RD0712) | 11930 | 1500 | Pinion fracture from manuf. crack | En24 | 1.00 | >1146 | En24 | 1.00 | >1146 |
| AVGRA 2DP (RD0710) | 17900 | 1500 | Pinion crack, PL, wheel pit | En36 | 1.00 | 1404[3] | En24 | 1.00 | 1404[3] |
| AVGRA 2DP (RD0708) | 8948 | 1500 | Pinion pit, wheel pit | En35 | 1.00 | 993 | En30B | 1.00 | 983[3] |
| AVGRA 2DP (RD0707) | 14914 | 1500 | Unfailed | En36 | 1.00 | >1282 | En36 | 1.00 | >1282 |
| NAVGRA 6DP (76/8) | 7457 | 1500 | Wheel crack, PL | En36 | 1.00 | >796 | En40B | 0.86 | 907[3] |
| NAVGRA 4DP (76/8) | 1185 | 1500 | Wheel crack, PL | En36 | 1.00 | >1168 | En40B | 0.79 | 1453 |
| NAVGRA 2DP (68/1) | 16405 | 1500 | Pinion exfoliation | En40C | 0.70 | 2073 | En9 | 1.00 | >1463 |
| AVGRA 6DP (W15) | 6711 | 600 | Wheel crack, root | En36A | 1.00 | >893 | En24 | 1.00 | 893 |
| AVGRA 3DP (W14) | 8359 | 6000 | Pinion crack, PL | En36 | 1.00 | 1243[3] | Nitralloy | 0.74 | >1680 |
| NAVGRA 8 mod(69/5) | 11282 | 6000 | Unfailed | En36 | 1.00 | >1407 | En40B | 0.75 | >1876 |
| NAVGRA 12DP (68/14) | 902 | 5200 | Wheel pit | En40B | 1.00 | >985 | En40B | 1.00 | 985[3] |
| NAVGRA 2DP (77/6) | 25500 | 1500 | Wheel crack after scuffing | En36 | 1.00 | >2255 | En36 | 1.00 | >2255 |

Notes:

1. En35 and 36, Carburised and hardened; En40, Nitrided; En24 and 9, Induction hardened; En30B, Through hardened to 70/75 T/in$^2$.

2. $\sigma_{HD}\, Z_G$ calculated from the failure load and factors

$$\sigma_{HD}\, Z_G = \frac{6181\, Z_H\, Z_E\, Z_\varepsilon}{Z_L\, Z_V\, Z_R\, Z_W\, Z_c} \sqrt{\frac{P_{Hfail}\,(u+1)\,K_A\,K_V\,K_{Ha}\,K_{H\beta}}{b\,d_{w1}^2\,n\,u}}$$

3. Result not included for reasons given